

How does sensor-wise N-BANDS relate to the of area of feasible solutions?

Tomass Andersons^a, Alejandro C. Olivieri^b, Mathias Sawall^a, Martina Beese^{a,c}, Klaus Neymeyr^{a,c}

^aInstitut für Mathematik, Universität Rostock, Ulmenstrasse 69, 18057 Rostock, Germany

^bDepartamento de Química Analítica, Facultad de Ciencias Bioquímicas y Farmacéuticas, Universidad Nacional de Rosario, Instituto de Química de Rosario (IQUIR-CONICET), Suipacha 531, Rosario S2002LRK, Argentina.

^cLeibniz-Institut für Katalyse, Albert-Einstein-Strasse 29a, 18059 Rostock, Germany

Abstract

Background: The method of sensor-wise N-BANDS aims to compute the envelope of the range of the feasible concentration profiles and the envelope of the range of the feasible spectral profiles. These envelopes are obtained by a sensor-wise maximization and minimization for each chemical species. They describe the rotational ambiguity which can also be explored by the area of feasible solutions. In this paper the results of sensor-wise N-BANDS are compared with the area of feasible solutions.

Results: Profiles in which sensor-wise N-BANDS takes point-wise extrema are shown to correspond to the boundary of the area of feasible solutions.

Significance: Sensor-wise N-BANDS is proven to correctly describe certain extremal AFS properties without any restrictions on the number of chemical species.

Key words: Sensor-wise N-BANDS, multivariate curve resolution, area of feasible solutions.

1. Introduction

Multivariate Curve Resolution (MCR) has its origin in analytical chemistry. The goal of MCR methods is to find an approximate factorization $D = CS^T + E$ of a given $k \times n$ spectral data matrix $D \in \mathbb{R}^{k \times n}$ into the nonnegative concentration factor $C \in \mathbb{R}^{k \times s}$ and the nonnegative spectral factor $S \in \mathbb{R}^{n \times s}$ where s is the number of chemical species. The matrix E is the error of the bilinear nonnegative factorization model and the entries of E should be close to zero. However, the nonnegative factors C and S are in most cases not uniquely determined, even if scaling is ignored. This non-uniqueness is known as rotational ambiguity (see, e.g., [4]). In analytical chemistry, additional constraints, e.g., monotonicity, unimodality or selectivity, are often added to the bilinear nonnegative factorization model to reduce the rotational ambiguity. However, under minimal constraints, the ambiguity can sometimes lead to very different solutions of the MCR problem. Therefore, it can be of interest to determine the rotational ambiguity present in a dataset.

This has been addressed with MCR-BANDS [17], N-BANDS [11] and sensor-wise N-BANDS (SW-N-BANDS) [9]. The goal of these methods is to describe the extent of rotational ambiguity by minimizing and maximizing the following functions (1),(2), and (3).

1. **MCR-BANDS:** The Signal Contributing Function (SCF)

$$f_j = \frac{\|C_{:,j}(S_{:,j})^T\|_F}{\|CS^T\|_F}, \quad j = 1, \dots, s \quad (1)$$

is used for constrained optimization, see also Eq. 6 in [17]. The same term in a different notation was given two years earlier in Eq. 8 in [3]. This paper uses the colon notation for elements of matrices, i.e., $C_{:,j}$ refers to the j -th column of the matrix C . As a further example, $T_{2:4,3}$ stands for the elements in the second, third, and fourth rows and third column of the matrix T .

2. **N-BANDS:** The contribution of S is optimized using the function

$$\hat{f}_j = \frac{\|S_{:,j}\|_1}{\|S\|_1}, \quad j = 1, \dots, s \quad (2)$$

and further constraints, e.g., for nonnegativity. Similarly, the procedure is applied to C to estimate the relative concentration uncertainty.

3. **SW-N-BANDS:** The constrained optimization is applied to each matrix element of S with the optimization function

$$\tilde{f}_{i,j} = \frac{|S_{i,j}|}{\|S\|_2}, \quad i = 1, \dots, n, \quad j = 1, \dots, s. \quad (3)$$

The same procedure is applied to the concentration factor C .

N-BANDS is an extension of MCR-BANDS that uses a simplified optimization function and is especially useful for noisy data. However, generally neither MCR-BANDS nor N-BANDS yields a complete envelope of the range of the feasible profiles, as discussed in [9]. By applying N-BANDS to each row and column of D , i.e., sensor-wise N-BANDS, the full envelope can be found. The main characteristic trait is that the envelope is usually not a feasible profile and does not directly represent the shapes of the feasible profiles. In contrast, the resulting upper and lower boundaries from the MCR-BANDS and N-BANDS methods are feasible profiles. Therefore, they are generally not equal to the full envelope of all feasible profiles, but may be more indicative of the shape of the feasible profiles.

A different approach to the rotational ambiguity is based on a low-dimensional representation of the solutions (see [7, 1, 13, 15]). Each feasible pure component profile has a corresponding point in an $(s - 1)$ -dimensional space (U -space or V -space), and the ambiguity is represented by the Area of Feasible Solutions (AFS). The U - and V -space is given by the vectors from the singular value decomposition (SVD) of $D \in \mathbb{R}^{k \times n}$. The truncated SVD is sufficient for this and is denoted by $U \in \mathbb{R}^{k \times s}$, $\Sigma \in \mathbb{R}^{s \times s}$ and $V \in \mathbb{R}^{n \times s}$. For example, a vector $x \in \mathbb{R}^{(s-1)}$ in V -space corresponds to a scaled spectrum $q \in \mathbb{R}^n$ if and only if $q = V_{:,1} + V_{:,2:s}x$. For simplicity, the focus of this paper is on the V -space, but all statements are connected to the U -space by duality, see, e.g., [5, 8]. Furthermore, we focus on the case $s = 3$, i.e., the case with three chemical species, because then the U - and V -space is a plane.

In this paper the connection between these two approaches is discussed by comparing the AFS and the V -space representations of the profiles that point-wise determine the SW-N-BANDS envelope, see also [12, 10]. This can help to answer some important questions, such as how the low-dimensional representations of SW-N-BANDS and AFS compare, and how well an SW-N-BANDS solution describes the rotational ambiguity compared to the AFS representation of the factor ambiguity. See also Fig. 1 as an example of the comparison of the available ‘‘information’’ on the feasible profiles. Each point in the plots corresponds to a feasible profile, and SW-N-BANDS can only produce profiles that point-wise minimize or maximize the function (3). Therefore, these results only represent a part of the AFS.

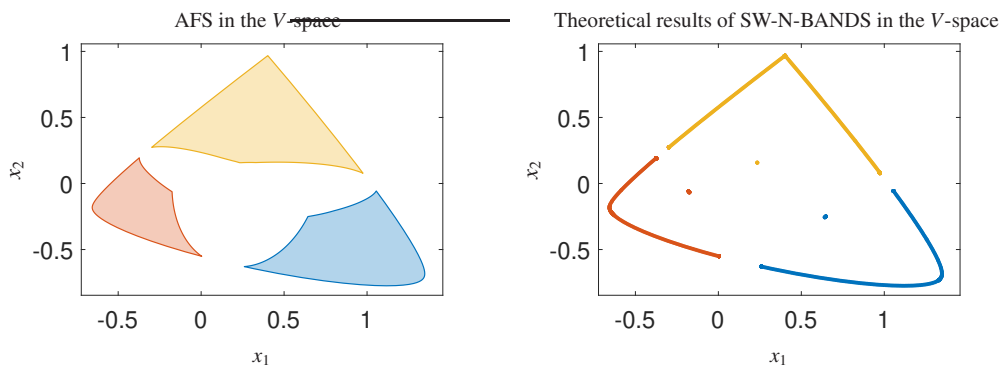


Figure 1: The ‘‘information’’ on the possible factorizations is shown in the V -space: the AFS (left) and the possible results discovered by SW-N-BANDS (right). Not all the points on the right side are included in the actual result from SW-N-BANDS as it depends on the number of sensors. The right figure is an example for the set \mathcal{M}^* from Def. 3.1.

1.1. The datasets

All examples in this paper are based on dataset 1, see Fig. 2. It is a simulated, noise-free dataset, which represents the reaction kinetics $\mathbf{X} \rightarrow \mathbf{Y} \rightarrow \mathbf{Z}$. Dataset 1 is based on `example2.m` from FACPACK [14] with 0.2 added to each

entry of the matrix D . The added constant inflates the AFS and helps to visualize both the main statement of this paper and the non-convexity of the AFS subsets. The simulated dataset consists of 21 time steps over 101 channels.

Dataset 2 is an experimental FT-IR dataset from the rhodium-catalyzed olefin hydroformylation, discussed in [6]. The absorption of the olefin species, the hydrido complexes and the acyl complex is given over the reaction time from 4.7 min to 883.6 min with 850 spectra over 645 channels in the wavenumber interval $[1962.3, 2117.6] \text{ cm}^{-1}$. The reference concentration profiles are obtained by kinetic hard-modeling analysis. An SW-N-BANDS analysis of this dataset is also presented in [10].

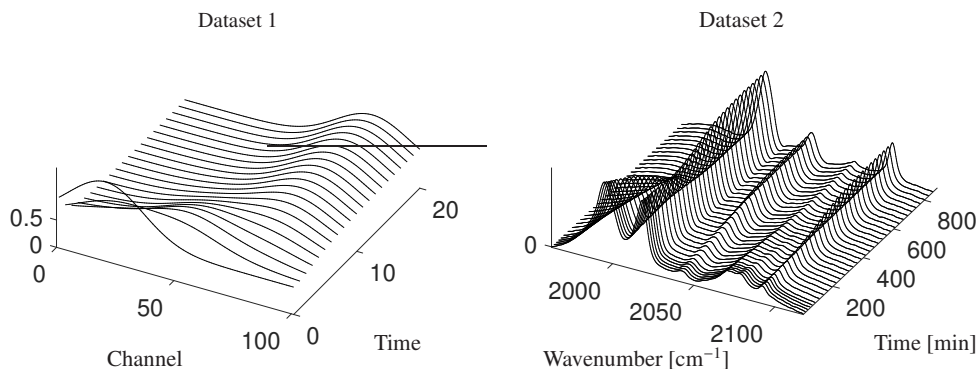


Figure 2: This paper includes the SW-N-BANDS analysis of a simulated dataset (left) and an experimental dataset (right).

2. Theoretical background

2.1. The AFS

Next, we give a brief summary of the important variables for the construction of the AFS, see [15] for further details and explanations. The rotational ambiguity of the factorization problem can be represented by the AFS and can be computed using the truncated SVD $D = U\Sigma V$. Then an inner polygon (also known as INNPOL and defined as $\mathcal{I} = \text{convhull}(\{a_i \in \mathbb{R}^{s-1}, i = 1, \dots, k\})$ with data representing points $a_i = ((U\Sigma)_{i,2:s}/(U\Sigma)_{i,1})^T$) and an outer polygon (also known as FIRPOL and defined as $\mathcal{F} = \{x \in \mathbb{R}^{s-1}, (1, x^T)V^T \geq 0\}$) are calculated. They give the inner and outer boundaries for polygons representing nonnegative factorizations. All feasible pure component profiles are represented by the AFS

$$\mathcal{M} = \left\{ x \in \mathbb{R}^{s+1} : \text{exists } T \in \mathbb{R}^{s \times s} \text{ with } T_{:,1} = \mathbf{1}, T_{1,2:s} = x^T, \text{rank}(T) = s, U\Sigma T^{-1} = C \geq 0, VT^T = S^T \geq 0 \right\},$$

where $\mathbf{1}$ is the all-ones vector and the factors C and S are computed using a regular matrix T . We define individual isolated AFS subsets as \mathcal{M}_j for $j = 1, \dots, s$. Then

$$\mathcal{M} = \bigcup_{j=1}^s \mathcal{M}_j.$$

Each point x in the V -space corresponds to a profile $w(x)$ which can be computed with $w(x) = (1, x^T)V^T$. By evaluating the profiles for each of the nodes of a fine grid of points covering the isolated AFS subsets, a good approximation of the envelope of the range of feasible profiles can be obtained, see Fig. 3 for an example.

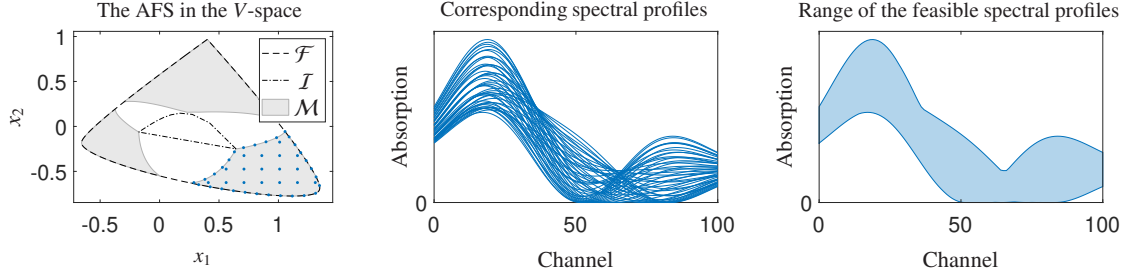


Figure 3: Computing the envelope of the range of feasible profiles from the AFS. An example of a grid (blue dots) on one isolated subset of the AFS (left) and the corresponding spectral profiles for one chemical species (middle). The maximum and minimum values for each channel represent the boundaries of the envelope (right). The finer the grid, the more accurate the representation of the the range of the feasible spectral profiles.

2.2. Sensor-wise N-BANDS

SW-N-BANDS approximates the minimum and maximum values for each entry in the factor matrices C and S under the nonnegativity constraints and scaling. Each point-wise extremum is associated with at least one profile in which the extremum is attained. This results in $2ks$ profiles for C and $2ns$ profiles for S , and each of these profiles achieves either a minimum or a maximum among all feasible profiles for a chemical species and a specific channel or time step, i.e., they are sensor-wise extremal profiles in this context. All calculated maxima and minima contribute point-wise to the envelopes of the ranges of the feasible profiles. The boundaries of these bands usually do not form feasible profiles, but there exists a feasible profile for each point on the envelope. Numerical errors can result from failed optimizations, large optimization tolerances, or noise. Such errors distort the results derived for the noise-free case, which is analyzed in the theoretical part of this paper. For example, the effect of noise is explained in [10].

The optimization problem is stated over a regular matrix \tilde{T} which represents the rotational ambiguity and reduces the number of variables in the optimization. The matrix \tilde{T} is applied to a feasible initial factorization $C_{\text{init}}S_{\text{init}}^T = D = C_{\text{init}}\tilde{T}^{-1}\tilde{T}S_{\text{init}}^T$, which can originate from MCR-ALS [16], for example.

Definition 2.1. *The optimization problem underlying SW-N-BANDS is given by*

$$\begin{cases} \min_{\tilde{T}} \frac{|S_{ij}|}{\|S\|_2} \\ \max_{\tilde{T}} \frac{|S_{ij}|}{\|S\|_2} \end{cases}, \text{ for each } i = 1, \dots, n \text{ and each } j = 1, \dots, s,$$

where $S^T = \tilde{T}S_{\text{init}}^T \geq 0$, $C = C_{\text{init}}\tilde{T}^{-1} \geq 0$, $\tilde{T}_{jj} = 1$ for each $j = 1, \dots, s$.

The same procedure is applied to C to obtain envelopes for the concentration profiles. Starting from an identity matrix, the zero entries in the matrix \tilde{T} are replaced by values in the neighborhood of zero, e.g., in the interval $[-1, 1]$. See [9] for more details.

The V -space representation uses a different scaling, and the profiles are given as a linear combination of the columns of V . The resulting profiles are scaled so that the contribution of the first singular vector is one. Only then, they have a V -space representation and can be compared with the AFS in the V -space. The V -space representation x of a spectral profile w is computed by $x = ((V_{:,2:s})^T w) / ((V_{:,1})^T w) \in \mathbb{R}^{s-1}$.

3. SW-N-BANDS takes its sensorwise extrema in the points of tangency of the AFS

In this section, we show that the profiles that solve the sensor-wise N-BANDS minimization or maximization problem are attained in *points of tangency* of the AFS. A point of tangency x is a point on the boundary of a set (with a piecewise smooth boundary) such that a tangent line (in 2D) or a tangent plane (in higher dimensions) running through the point x does not intersect the set. Fig. 4 illustrates the points of tangency for the three isolated subsets of a two-dimensional AFS. Next, we consider a simple property of the set of points of tangency \mathcal{M}_j^* , applied to isolated subsets \mathcal{M}_j of the AFS (this property is closely related to the so-called supporting hyperplane theorem in geometry [2]).

Lemma 3.1. *The set of points of tangency \mathcal{M}_j^* of an isolated subset \mathcal{M}_j of the AFS can be represented as*

$$\mathcal{M}_j^* = \mathcal{M}_j \cap \partial(\text{convhull}(\mathcal{M}_j)),$$

In words, the set \mathcal{M}_j^ is the intersection of \mathcal{M}_j with the boundary of the convex hull of \mathcal{M}_j .*

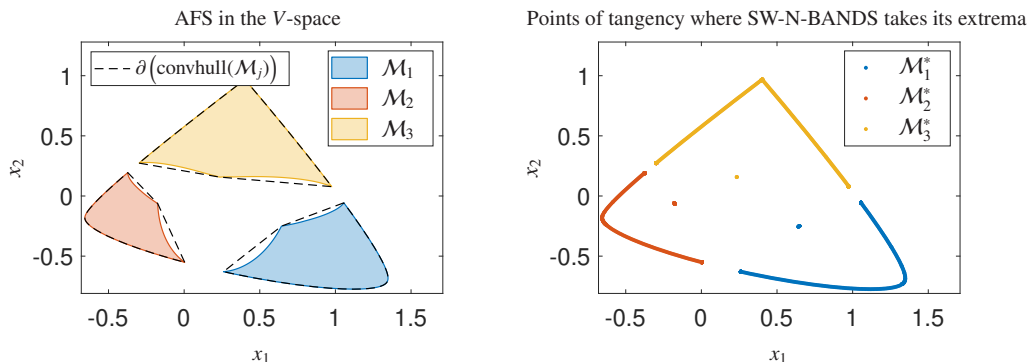


Figure 4: The construction of \mathcal{M}^* according to Lemma 3.1. The convex hulls of each isolated AFS subset \mathcal{M}_j are drawn by dashed lines (left). The right plot shows the three sets of points of tangency for the three subsets of the AFS.

The right plot in Fig. 4 illustrates individual sets \mathcal{M}_j^* of points of tangency in the V -space. This example demonstrates that concave regions of the boundary do not contain points of tangency. Next, we prove that all profiles in which SW-N-BANDS takes its extrema are represented by points of tangency in the V -space of the AFS.

Theorem 3.2. *The V -space representations of the profiles that sensor-wise contribute to the SW-N-BANDS envelopes are located in $\mathcal{M}^* = \bigcup_{j=1}^s \mathcal{M}_j^*$, namely the set union over all subset indexes j .*

Proof. SW-N-BANDS determines the extrema of $S_{i,j}$ according to Eq. (3) under nonnegativity and scaling constraints for $i = 1, \dots, n$ and $j = 1, \dots, s$. Without loss of generality any spectral profile $S_{:,j}$ can be assumed to be scaled in a way that it can be written as $S_{:,j} = V \begin{pmatrix} 1 \\ x \end{pmatrix}$ where the vector $x \in \mathbb{R}^{s-1}$ is the associated V -space representation in the AFS space. For the i th sensor/channel the representation is

$$S_{i,j} = V_{i,1} + x_1 V_{i,2} + \dots + x_{s-1} V_{i,s}. \quad (4)$$

The question is where $S_{i,j}$ takes its minimum and maximum with respect to a variation of the feasible $x \in \mathcal{M}_j$, namely the AFS subset of the j th chemical species. The optimization problem for (4) can be reduced to finding the minimum and maximum of the inner product $v^T x$ with $v = (V_{i,2}, \dots, V_{i,s})^T$ and $x \in \mathcal{M}_j$. The level sets $\mathcal{L}_\eta = \{x \in \mathbb{R}^{s-1} : v^T x = \eta - V_{i,1}\}$ of the inner product $v^T x$ are given by parallel affine planes all with the normal vector v . These level sets for all $\eta \in \mathbb{R}$ cover the entire space \mathbb{R}^{s-1} where the shifted η values increase/decrease linearly in the direction of $\pm v$. Only those level sets are important that have a nonempty intersection with \mathcal{M}_j (as otherwise no feasible solution is represented). Since \mathcal{M}_j is a closed and bounded set [8], there is a unique η_{\min} and a unique η_{\max} for which the level sets still touch \mathcal{M}_j . See Fig. 5 for an illustration where the hyperplanes in 2D are straight lines. Depending on whether the hyperplane touches \mathcal{M}_j in one or more points, the vector x on the boundary of \mathcal{M}_j is unique or not. By construction, x is a point of tangency to \mathcal{M}_j which proves that $x \in \mathcal{M}_j^*$. \square

The proof of Thm. 3.2 illustrates the origin and meaning of the set \mathcal{M}^* representing the SW-N-BANDS envelopes. The maximum and minimum values for each sensor can be explained by a pair of parallel hyperplanes, see Fig. 5. All of these hyperplanes are shown in Fig. 6 for both the lower and upper boundaries of the envelope.

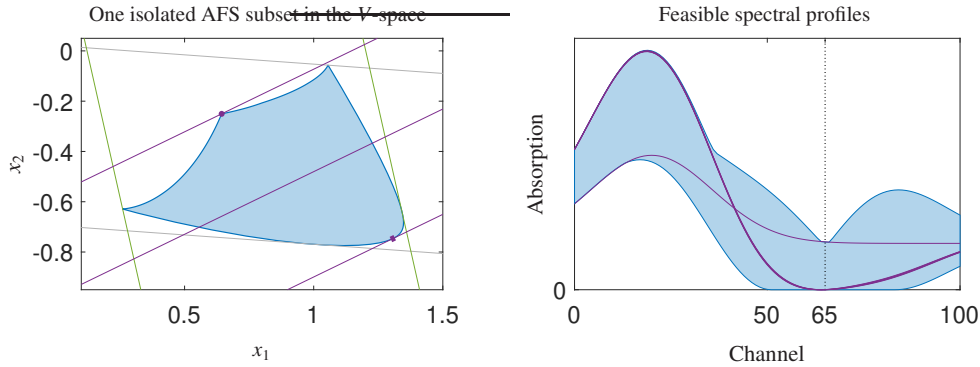


Figure 5: Geometric construction of the sensor-wise extremal profiles for $S_{65,1}$ shown with an isolated AFS subset and the corresponding envelope of the feasible profiles. Left: the isolated AFS subset \mathcal{M}_1 of the chemical species with index $j = 1$ (blue). Purple lines illustrate the hyperplanes from the proof of Thm. 3.2 for the channel (sensor) $i = 65$ and $\eta \in \{0.06905, 0.035, 0\}$ (from top to bottom). The spectral profiles that minimize or maximize at least one entry in $S_{65,1}$ are represented by purple dots. Other examples of hyperplanes are shown by gray and green lines. The gray lines show hyperplanes for $i = 58$ and $\eta \in \{0.10854, 0\}$ (from top to bottom). The green lines show two hyperplanes for $i = 75$ and $\eta \in \{0.11764, 0\}$ (from left to right). Right: the envelope of the feasible profiles corresponding to the isolated AFS subset \mathcal{M}_1 . The purple lines show the spectral profiles corresponding to the purple dots in the AFS, and they lie on the envelope for the 65th channel.

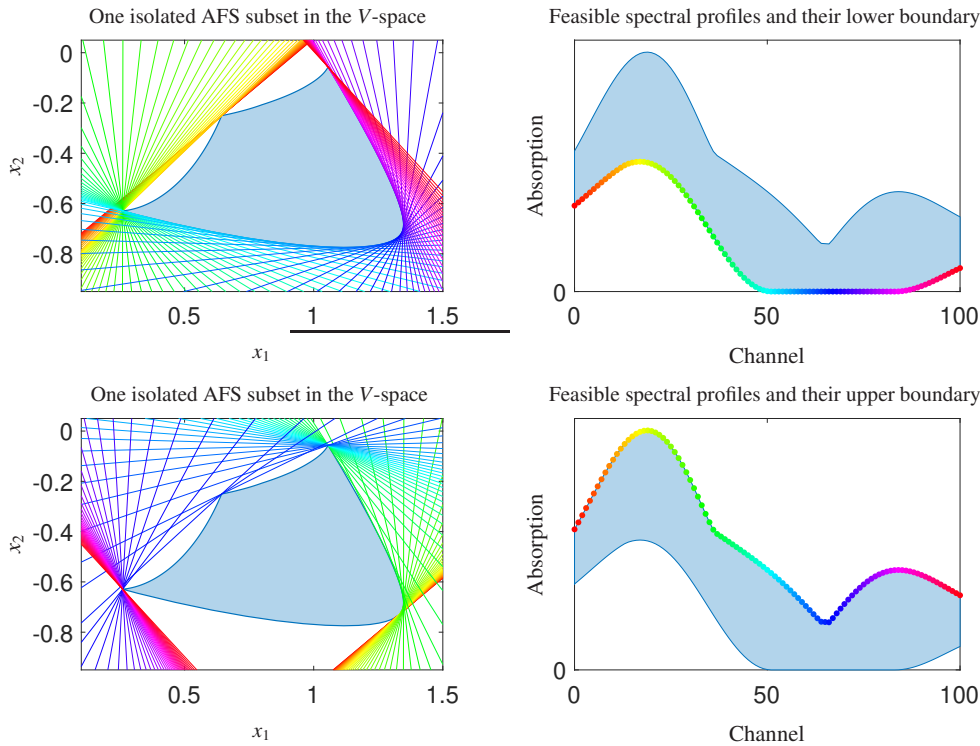


Figure 6: All channels (sensors), their minima (top plots) and maxima (bottom plots) in the AFS (left plots) and on the envelope of the feasible profiles (right plots) for \mathcal{M}_1 . The left plots show each hyperplane for $i = 1, \dots, n$ from the proof of Thm. 3.2 with $\eta = \eta_{\min,i}$ (top) and $\eta = \eta_{\max,i}$ (bottom). Each intersection of these hyperplanes with the AFS corresponds to a sensor-wise extremal profile in one of the right plots with the extreme value in the i th channel (sensor). The extreme values are plotted in the same color as the corresponding hyperplanes.

The results of the Thm. 3.2 as well as numerical SW-N-BANDS calculations can be verified with a short consideration. If a certain AFS is given, then \mathcal{M}^* and the SW-N-BANDS envelope can be constructed to check the results of the Thm. 3.2. Numerically, we can approximate the envelopes by covering the AFS with a (fine) grid and calculating the corresponding spectral profile of each grid point, see Fig. 3. Then we can determine which points from the grid maximize or minimize at least one entry in S . This usually overlaps with \mathcal{M}^* , however a problem can be constructed

where a point in \mathcal{M}^* does not correspond to a sensor-wise extremal profile. This does not contradict Thm. 3.2 and would only happen, if none of the shifted hyperplanes (as shown in Fig. 6) touches a part of \mathcal{M}^* . This is unlikely to happen in practice because the dataset typically contains enough sensors with different information to introduce variability in the hyperplanes.

In [18] it is shown that SW-N-BANDS can be complemented with the idea of essential points. Essential points can be defined as those data representing points that generate the convex hull of the inner polygons in U - and V -space. They can be roughly interpreted as a subset of the rows or columns of the matrix D that still generate the same inner and outer polygons. In this way, essential points make it possible to reduce the data dimension without changing the AFS in the original U - and V -space. In the context of SW-N-BANDS, the optimization problem of Def. 2.1 is applied only to the rows of S (index i) corresponding to the essential points, instead of all $i = 1, \dots, n$. Thm. 3.2 still holds, but \mathcal{M}^* is generated only by those hyperplanes that correspond to the essential points. Therefore, the construction as shown in Fig. 6 is reduced to only the essential hyperplanes and spectral channels, because the band boundaries of the others can be obtained implicitly. In [18] it is also discussed, how the concept of essential points can be applied to noisy data.

The final result of an SW-N-BANDS calculation is an envelope, whose upper and lower boundaries are generally not feasible profiles. Nevertheless, it is possible to make a statement about the shapes of the feasible profiles. Only those profiles in the envelope that are linear combinations of the singular vectors can be feasible. This is a useful rule of thumb, when trying to interpret the resulting envelopes. Unfortunately, this is not always true and the justification follows from another interesting property of the AFS: The AFS subsets are generally not convex, see, e.g., the left plot in Fig. 1. And in the right plot in Fig. 1, there are only a few points in the interior of \mathcal{F} (outer polygon shown e.g. in Fig. 3) because \mathcal{M}^* is defined by the boundary of the convex hull of each isolated AFS subset (shown in Fig. 4) and not by the boundary of the AFS itself. Therefore, $\mathcal{M} \subset \mathcal{M}^*$ and in general an AFS subset \mathcal{M}_j is not equal to the convex hull of the points of tangency \mathcal{M}_j^* (which represents the profiles in the envelope and is the result from SW-N-BANDS analysis). This explains the following property.

Remark 3.3. *There can be profiles in the column space of D that lie between the SW-N-BANDS envelope, but are not feasible.*

In other words, the envelope visualization of the rotational ambiguity may include some profiles that can be expressed by the singular vectors of D (i.e., they are in the same column space and in the V -space), but that are not in the AFS. See the green point and profile in Fig. 7. This means that AFS provides a more accurate description of the rotational ambiguity because it is possible to specify which profiles in the envelope are feasible. Nevertheless, the band representation is very useful because it directly visualizes the general shape of the band of feasible profiles.

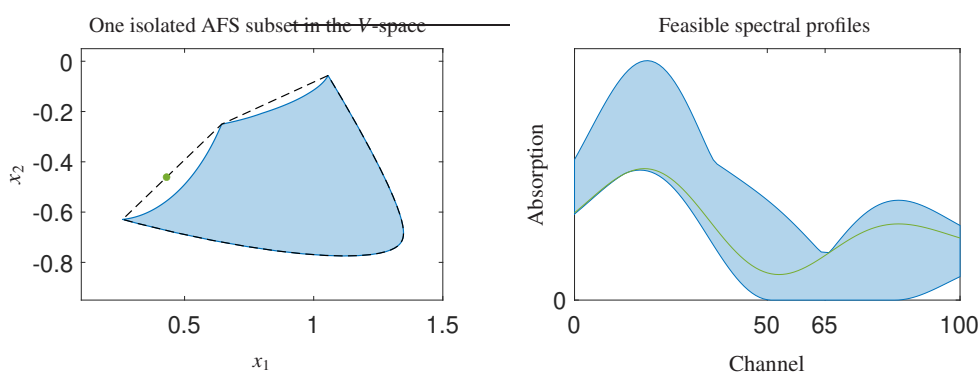


Figure 7: An example of a profile that is in the range of feasible profiles and in the V -space, but not in the AFS. Left: the isolated AFS subset for one chemical species (blue). The dashed lines indicate the boundary of the convex hull of the isolated AFS subset. The green point is located in the convex hull of the isolated AFS subset, but not in the AFS. Right: the envelope of the feasible profiles corresponding to the isolated AFS subset. The green profile corresponds to the green point in the left plot and is not a feasible profile.

4. Numerical results

4.1. Dataset 1

The example dataset is evaluated with SW-N-BANDS to compare how well it overlaps with the theoretically predicted results, see Fig. 8. The results of this example show a very good agreement with the theoretically predicted results in Fig. 1. SW-N-BANDS was performed with the `fmincon` SQP algorithm in `MATLAB`, with a better precision than the default and with the interval $[-1.45, 1.45]$ for the values of \bar{T} . For a matrix $S \in \mathbb{R}^{n \times 3}$ SW-N-BANDS results in most $6n$ profiles and corresponding points in the V -space. Therefore, there are much fewer points in Fig. 8 than the theoretically possible results in Fig. 1, which take into account that more than one spectral profile can minimize or maximize a particular entry in S .

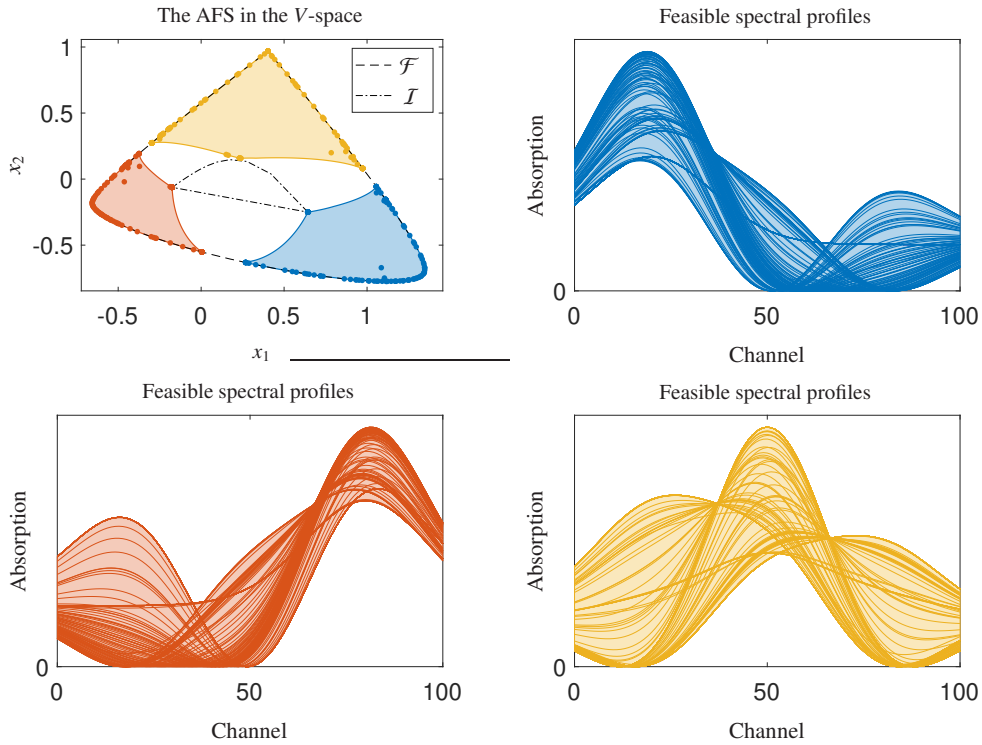


Figure 8: The results of a numerical evaluation of SW-N-BANDS (points and profiles in saturated colors) and AFS (areas and envelopes in light colors) for the dataset 1. Top left: inner polygon \mathcal{I} , outer polygon \mathcal{F} , AFS \mathcal{M} (blue, red and yellow for the three chemical species) and V -space representations of the points resulting from SW-N-BANDS (corresponding colors). The three other plots each show the envelope of the feasible profiles corresponding to one isolated AFS subset (light color) and the sensor-wise extremal profiles from the numerical evaluation of SW-N-BANDS for this subset (individual profiles in saturated color).

4.2. Dataset 2

The experimental dataset also shows a good overlap between the SW-N-BANDS results and the AFS. Furthermore, there are only a few points that do not belong to the outer polygon \mathcal{F} as predicted by Thm. 3.2, see Fig 9. The red AFS subset gives a very clear illustration of this relationship. The results are presented for U -space, to illustrate that the duality concept can be applied to Thm. 3.2. In the case of noisy, experimental data, some slight differences can be explained by different approaches to dealing with the noise, as well as by unsuccessful optimization. The results slightly differ from those published in [10], due to the use of different noise levels. In this paper, AFS is computed with a noise level of 0.27% and SW-N-BANDS is computed with a noise level of 0.2%.

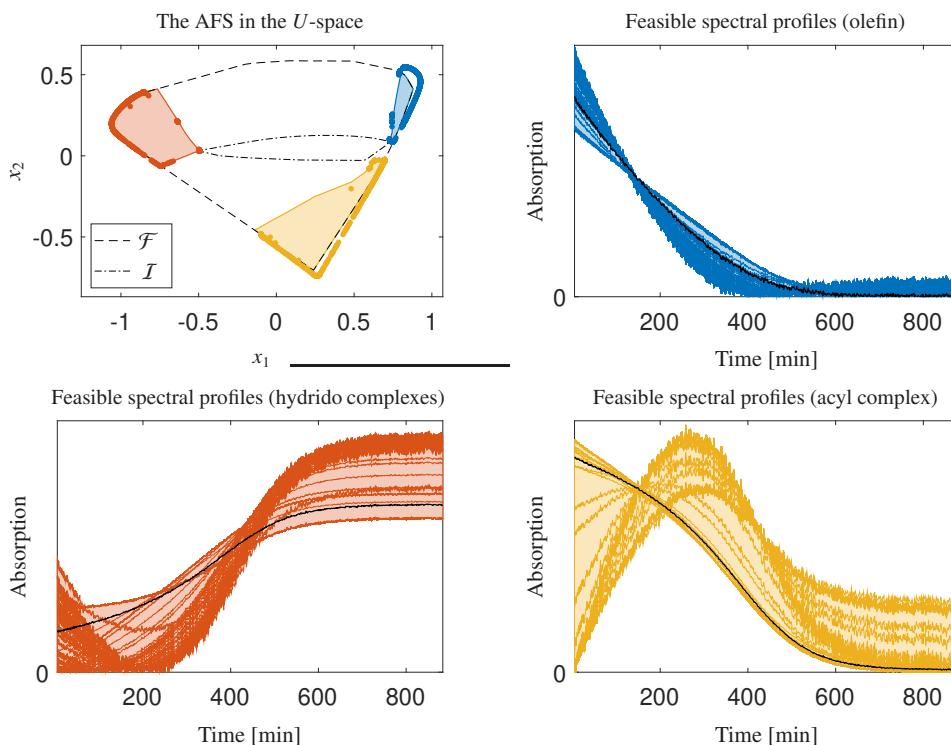


Figure 9: The results of a numerical evaluation of SW-N-BANDS (points and profiles in saturated colors) and AFS (areas and envelopes in light colors) for the dataset 2. Top left: inner polygon I , outer polygon F , AFS M (blue, red and yellow for the three chemical species) and V -space representations of the points resulting from SW-N-BANDS (corresponding colors). The three other plots each show the envelope of the feasible profiles corresponding to one isolated AFS subset (light color) and the sensor-wise extremal profiles from the numerical evaluation of SW-N-BANDS for this subset (individual profiles in saturated color). The black lines are the true profiles from kinetic hard-modeling.

5. Conclusion

It is a remarkable fact that the U - and V -space representations of the sensor-wise extremal profiles determined by the SW-N-BANDS are located on certain parts of the boundary of the AFS. These extremal profiles contribute point-wise to the envelopes of the ranges of the concentration and spectral profiles that represent the factor ambiguity of MCR problems. Their close relation to the AFS is formalized in this paper as follows: The results of SW-N-BANDS are represented by M^* , i.e., the intersection of the AFS and the boundary of the convex hull of each isolated AFS subset. However, SW-N-BANDS is designed for the cases of datasets, whose number of isolated AFS segments is equal to the number of chemical species. Even if there exists only one connected AFS subset, which is often the case for highly overlapping spectral data, SW-N-BANDS will still detect different envelopes and this is a problem for future research. Nevertheless, a major advantage of the SW-N-BANDS method is its adaptability to problems with a large number of chemical species, while the AFS method requires an $(s-1)$ -dimensional representation for s chemical species. That is very difficult for more than four chemical species, because it is hard to visualize and handle sets in more than three dimensions.

References

- [1] O.S. Borgen and B.R. Kowalski. An extension of the multivariate component-resolution method to three components. *Anal. Chim. Acta*, 174:1–26, 1985.
- [2] S.P. Boyd and L. Vandenberghe. *Convex optimization*. Cambridge Univ. Press, Cambridge, 8. printing edition, 2010.
- [3] P.J. Gemperline. Computation of the range of feasible solutions in self-modeling curve resolution algorithms. *Anal. Chem.*, 71(23):5398–5404, 1999.

- [4] A. Golshan, H. Abdollahi, and M. Maeder. Resolution of rotational ambiguity for three-component systems. *Anal. Chem.*, 83(3):836–841, 2011.
- [5] R.C. Henry. Duality in multivariate receptor models. *Chemom. Intell. Lab. Syst.*, 77(1-2):59–63, 2005.
- [6] C. Kubis, M. Sawall, A. Block, K. Neymeyr, R. Ludwig, A. Börner, and D. Selent. An operando FTIR spectroscopic and kinetic study of carbon monoxide pressure influence on rhodium-catalyzed olefin hydroformylation. *Chem.-Eur. J.*, 20(37):11921–11931, 2014.
- [7] W.H. Lawton and E.A. Sylvestre. Self modelling curve resolution. *Technometrics*, 13(3):617–633, 1971.
- [8] K. Neymeyr and M. Sawall. On the set of solutions of the nonnegative matrix factorization problem. *SIAM J. Matrix Anal. Appl.*, 39(2):1049–1069, 2018.
- [9] A.C. Olivieri. Estimating the boundaries of the feasible profiles in the bilinear decomposition of multi-component data matrices. *Chemom. Intell. Lab. Syst.*, 216:104387, 2021.
- [10] A.C. Olivieri, M. Sawall, K. Neymeyr, and R. Tauler. Noise effects on band boundaries in multivariate curve resolution of three-component systems. *Chemom. Intell. Lab. Syst.*, 228:104636, 2022.
- [11] A.C. Olivieri and R. Tauler. N-BANDS: A new algorithm for estimating the extension of feasible bands in multivariate curve resolution of multicomponent systems in the presence of noise and rotational ambiguity. *J. Chemom.*, 35(3):e3317, 2021.
- [12] R. Rajkó. Computation of the range (band boundaries) of feasible solutions and measure of the rotational ambiguity in self-modeling/multivariate curve resolution. *Anal. Chim. Acta*, 645(1–2):18–24, 2009.
- [13] R. Rajkó and K. István. Analytical solution for determining feasible regions of self-modeling curve resolution (SMCR) method based on computational geometry. *J. Chemom.*, 19(8):448–463, 2005.
- [14] M. Sawall and K. Neymeyr. *How to compute the Area of Feasible Solutions, A practical case study and users' guide to FAC-PACK*, volume in Current Applications of Chemometrics, ed. by M. Khanmohammadi, chapter 6, pages 97–134. Nova Science Publishers, New York, 2014.
- [15] M. Sawall, H. Schröder, D. Meinhardt, and K. Neymeyr. On the ambiguity underlying multivariate curve resolution methods. In S. Brown, R. Tauler, and B. Walczak, editors, *Comprehensive Chemometrics: Chemical and Biochemical Data Analysis*, pages 199–231. Elsevier, Cambridge, MA, 2020.
- [16] R. Tauler. Multivariate curve resolution applied to second order data. *Chemom. Intell. Lab. Syst.*, 30(1):133–146, 1995.
- [17] R. Tauler. Calculation of maximum and minimum band boundaries of feasible solutions for species profiles obtained by multivariate curve resolution. *J. Chemom.*, 15(8):627–646, 2001.
- [18] S. Vali Zade, M. Sawall, K. Neymeyr, A.C. Olivieri, R. Tauler, and H. Abdollahi. Feasible band boundaries computation in bilinear matrix decomposition using essential data. *Anal. Chim. Acta*, 1336:343538, 2025.